Yip1 domain family, member 6 (Yipf6) mutation induces spontaneous intestinal inflammation in mice

Katharina Brandl[a], Wataru Tomisato[a,b], Xiaohong Li[a,b], Christina Neppl[a], Elaine Pirie[a], Werner Falk[c], Yu Xia[a], Eva Marie Y. Moresco[a], Roberto Baccala[d], Argyrios N. Theofilopoulos[d], Bernd Schnabl[e], and Bruce Beutler[a,b,1]

[a]Department of Genetics, The Scripps Research Institute, La Jolla, CA 92037; [b]Center for Genetics of Host Defense, University of Texas Southwestern Medical Center, Dallas, TX 75390; [c]Department of Internal Medicine I, University of Regensburg, 93053 Regensburg, Germany; [d]Department of Immunology and Microbial Science, The Scripps Research Institute, La Jolla, CA 92037; and [e]Department of Medicine, University of California San Diego, La Jolla, CA 92093

Contributed by Bruce Beutler, June 19, 2012 (sent for review May 18, 2012)

Using an environmentally sensitized genetic screen we identified mutations that cause inflammatory colitis in mice. The X-linked *Klein-Zschocher* (*KLZ*) mutation created a null allele of *Yipf6*, a member of a gene family believed to regulate vesicular transport in yeast, but without known functions in mammals. Yipf6 is a five transmembrane-spanning protein associated with Golgi compartments. *Klein-Zschocher* mutants were extremely sensitive to colitis induced by dextran sodium sulfate (DSS) and developed spontaneous ileitis and colitis after 16 mo of age in specific pathogen-free housing conditions. Electron microscopy, gene expression, and immunocytochemistry analyses provided evidence that impaired intestinal homeostasis stemmed from defective formation and secretion of large secretory granules from Paneth and goblet cells. These studies support a tissue- and organ-specific function for Yipf6 in the maintenance of intestinal homeostasis and implicate the orthologous human gene as a disease susceptibility locus.

The epithelium of the gastrointestinal tract is occasionally subject to injury by toxigenic enteric pathogens and perhaps on occasion by microscopic particulates capable of wounding cells. However, homeostatic mechanisms normally restore the status quo ante, so that dysfunction is short-lived. These mechanisms are activated both within epithelial cells of the gut and within cells of the immune system. Their failure may lead to a chronic disease state, recognized clinically as inflammatory bowel disease (IBD).

To identify genes with nonredundant function in intestinal homeostasis, we used an environmentally sensitized genetic screen, in which mice with both homozygous and heterozygous germline mutations induced by *N*-ethyl-*N*-nitrosourea (ENU) were exposed for 1 wk to 1% (wt/vol) DSS in drinking water, a concentration harmless to wild-type animals. We anticipated that a fraction of the mutations disclosed by DSS hypersensitivity would cause spontaneous disease and could therefore provide new animal models of IBD. Furthermore, these genetically defined models could identify candidate genes for IBD, disclose important mechanisms for this disease, and implicate potential targets for therapy.

Results and Discussion

Approximately 6,000 mice were screened by daily weighing and outliers displaying extreme weight loss were retrieved for further study. A total of 16 transmissible mutations causing hypersensitivity to DSS were detected (Fig. 1*A*). Of these, 5 were identified. Four affected the genes encoding Tlr9, Aqp3, and Muc2 (two alleles) and appeared to be necessary for restoration of epithelial integrity after wounding by DSS. In particular, previous studies showed that failure of epithelial integrity is sensed by Toll-like receptors on epithelial cells, leading to the induction of amphiregulin and epiregulin, members of the EGF ligand family (1). Wound closure additionally requires signaling via the EGF receptor pathway (1), water transport via aquaporin 3 (2), and an intact unfolded protein response dependent on Mbtps1, also known as the site-1 protease (3). Relatively common mutations affecting the structure of Mucin-2 also enhance susceptibility to colitis, evidently by increasing ER stress (4), and do so in a semidominant fashion.

The fifth mutant, called *Klein-Zschocher* (*KLZ*) (after the town named in J. S. Bach cantata BWV 212), showed severe weight loss after 1% DSS administration (Fig. 1*B*); both hemizygous males and homozygous females displayed the phenotype clearly. Hematoxylin and eosin (H&E) staining of histologic sections from colons showed dramatic leukocyte recruitment and crypt loss in the mutant strain compared with wild-type mice after 7 d of 1% DSS (Fig. 1*C*). Administration of a higher DSS dose resulted in rapid weight loss and lethality in all mutant mice 7 to 9 d after onset of treatment (Fig. 1*D*). Intestinal permeability was increased by 85% in mutant relative to wild-type mice, suggesting epithelial barrier dysfunction in the absence of DSS administration (Fig. 1*E*). The X-linked *Klein-Zschocher* phenotype was first observed at the age of 6 wk (the earliest age at which mice were tested), and was fully penetrant on the C57BL/6J background.

To test whether primary epithelial dysfunction is responsible for increased susceptibility to DSS-induced colitis in *Klein-Zschocher* mice, bone marrow chimeric mice were generated in which donors and/or recipients were either wild-type (CD45.1) or *Klein-Zschocher* mutant (CD45.2). Significant weight loss (Fig. 1*F*), destruction of colonic epithelial architecture (Fig. S1*A*), and shortening of the colon (Fig. S1*B*) were observed in mutant mice receiving wild-type bone marrow, but not in wild-type mice receiving mutant bone marrow. Thus, the *Klein-Zschocher* mutation operates in nonhematopoietic cells to permit the hypersensitivity to DSS.

We hypothesized that *Klein-Zschocher* mutants might also develop spontaneous intestinal inflammation. Under specific pathogen-free housing conditions, no pathology was observed through at least 1 y of age. However, 16-mo-old mutants displayed shortening of the colon, indicating chronic edema and inflammation (Fig. 1*G*), and numerous cellular defects of the lamina propria and epithelium in the small intestine and colon (Fig. 1*H*). These cellular defects included patchy transmural neutrophilic and lymphocytic infiltrates in the lamina propria of the small intestine (asterisks, Fig. 1*H*, *b* and *d*), villus fusion (arrows, Fig. 1*H*, *b* and *d*), and thickening of the submucosa (arrow, Fig. 1*H*, *c*). Colonic inflammation (Fig. 1*H*, *f*–*h*) consisted

Author contributions: K.B., W.F., R.B., A.N.T., B.S., and B.B. designed research; K.B., W.T., X.L., C.N., E.P., W.F., and B.S. performed research; K.B., Y.X., E.M.Y.M., and B.B. analyzed data; and K.B., E.M.Y.M., R.B., A.N.T., and B.B. wrote the paper.

The authors declare no conflict of interest.

Data deposition: The *Klein-Zschocher* strain reported in this paper has been deposited in the Mutant Mouse Regional Resource Center [ID no. 034313-UCD (C57BL/6J-*Yipf6*^{m1Btlr}/Mmucd)].

[1]To whom correspondence should be addressed. E-mail: Bruce.Beutler@UTSouthwestern.edu.

This article contains supporting information online at www.pnas.org/lookup/suppl/doi:10.1073/pnas.1210366109/-/DCSupplemental.

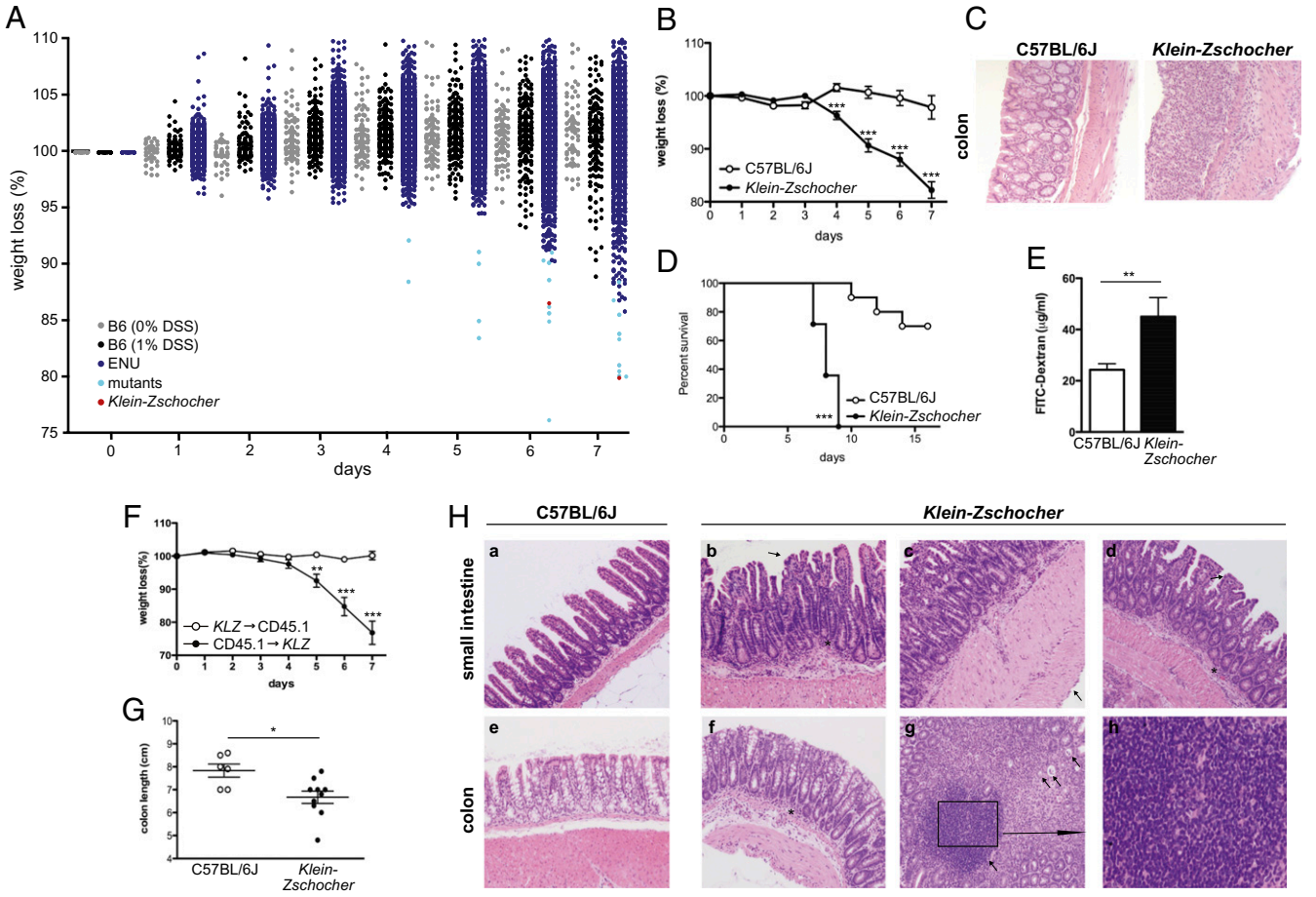

Fig. 1. Increased susceptibility of *Klein-Zschocher* mice to induced colitis. (*A* and *B*) Percent weight change of mice given 1% DSS in drinking water for 7 d. (*A*) Approximately 6,000 mutagenized mice (ENU) were screened; ~2,300 are shown here. WT (C57BL/6J) mice receiving 1% DSS (n = ~200) or 0% DSS (n = ~100) served as controls. Strains with transmissible mutations (light blue); *Klein-Zschocher* (red). (*B*) n = 8–9 each group including hemizygous males and homozygous females; for days 1 and 2, only three mice from each group were weighed. Unpaired t test, ***$P < 0.0005$. (*C*) Representative photomicrographs (magnification 200×; H&E) of colons from mice at day 7 of 1% DSS administration. (*D*) Survival of mice after administration of 4% DSS. n = 8–10 each group; log rank (Mantel–Cox) test, ***$P < 0.0001$. (*E*) Plasma FITC-dextran concentrations in naive mice 4 h following oral gavage. n = 4–7 each group; unpaired t test, **$P = 0.0091$. (*F*) Percent weight change of BM chimeric mice upon administration of 1% DSS in the drinking water. *KLZ*, *Klein-Zschocher*. n = 4–5 each group; unpaired t test, **$P < 0.005$, ***$P < 0.001$. (*G*) Colon length of 16-mo-old mice. n = 6–10 males each group; unpaired t test, *$P < 0.05$. (*H*) Representative photomicrographs (H&E; *a*–*g*, magnification 100×; *h*, magnification 400×) showing pathology of distal small intestines and colons from 16-mo-old male mice. See text for description. All error bars represent SEM.

of mild lamina propria infiltration of neutrophils and lymphocytes (asterisk, Fig. 1*H*, *f*), crypt abscesses (arrows, Fig. 1*H*, *g*), and mucosal lymphoid aggregates (Fig. 1*H*, *Inset* box in *g*; *h*).

To understand the pathogenesis of spontaneous intestinal inflammation and increased susceptibility to induced colitis in *Klein-Zschocher* mice, naive mutants were examined for intestinal abnormalities. Although overall morphology of the small intestine and colon was normal (Fig. 2 *A*–*D*), Paneth and goblet cells were reduced in number, contained less stainable material, and were oddly shaped (Fig. 2 *E*–*H*). The mucin content of the colon was also drastically reduced (Fig. 2 *G* and *H*). Electron microscopy revealed diminutive and disorganized granules in Paneth cells (Fig. 2 *I*, *J*, *M*, and *N*). In goblet cells, mucin granules were slightly smaller in size and more variable in electron density than in WT mice (Fig. 2 *K*, *L*, *O*, and *P*). Gene expression of the defensin peptides cryptidin-3, -4, -5, and lysozyme was significantly reduced, consistent with the lower numbers of Paneth cells and granules (Fig. 2*Q*). Notably, expression of the ER stress marker Chop was normal, showing that the reduced numbers of Paneth cells is not caused by increased ER stress and cell death (5) (Fig. 2*Q*). TUNEL assays also revealed normal levels of apoptosis of Paneth and goblet cells. Consistent with mRNA data, lysozyme protein levels were significantly reduced in the small intestine (Fig. 2*R*). These findings suggest that spontaneous and induced colitis in *Klein-Zschocher* mice stem from alterations in the granule exocytosis pathway of intestinal epithelial cells. The Paneth cell phenotype we observed was similar to that of mice with a hypomorphic mutation of *Atg16l1* (6); however, no significant change in the level of autophagy protein LC3, encoded by *Map1lc3a*, could be detected in *Klein-Zschocher* mice.

The *Klein-Zschocher* mutation was mapped to chromosome X with a LOD score of 17.4 (Fig. 3*A*). Analysis of 79 meioses confined the mutation to a critical region bounded by DXMit114 and DXMit169 (95.34–97.952 Mb), comprising about 1 thousandth of the genome (Fig. 3*B*). Whole-genome SOLiD sequencing of mutant DNA revealed a single hemizygous coding/splicing mutation within the critical region: a T-to-A transversion at position 3002 (Fig. 3*C*) of the genomic DNA sequence of *Yipf6*, which encodes a 236-amino-acid protein (Fig. 3*D*). The mutation lies in the splice acceptor site of intron 3 of the 7-exon gene, and affects a thymine base five nucleotides upstream from

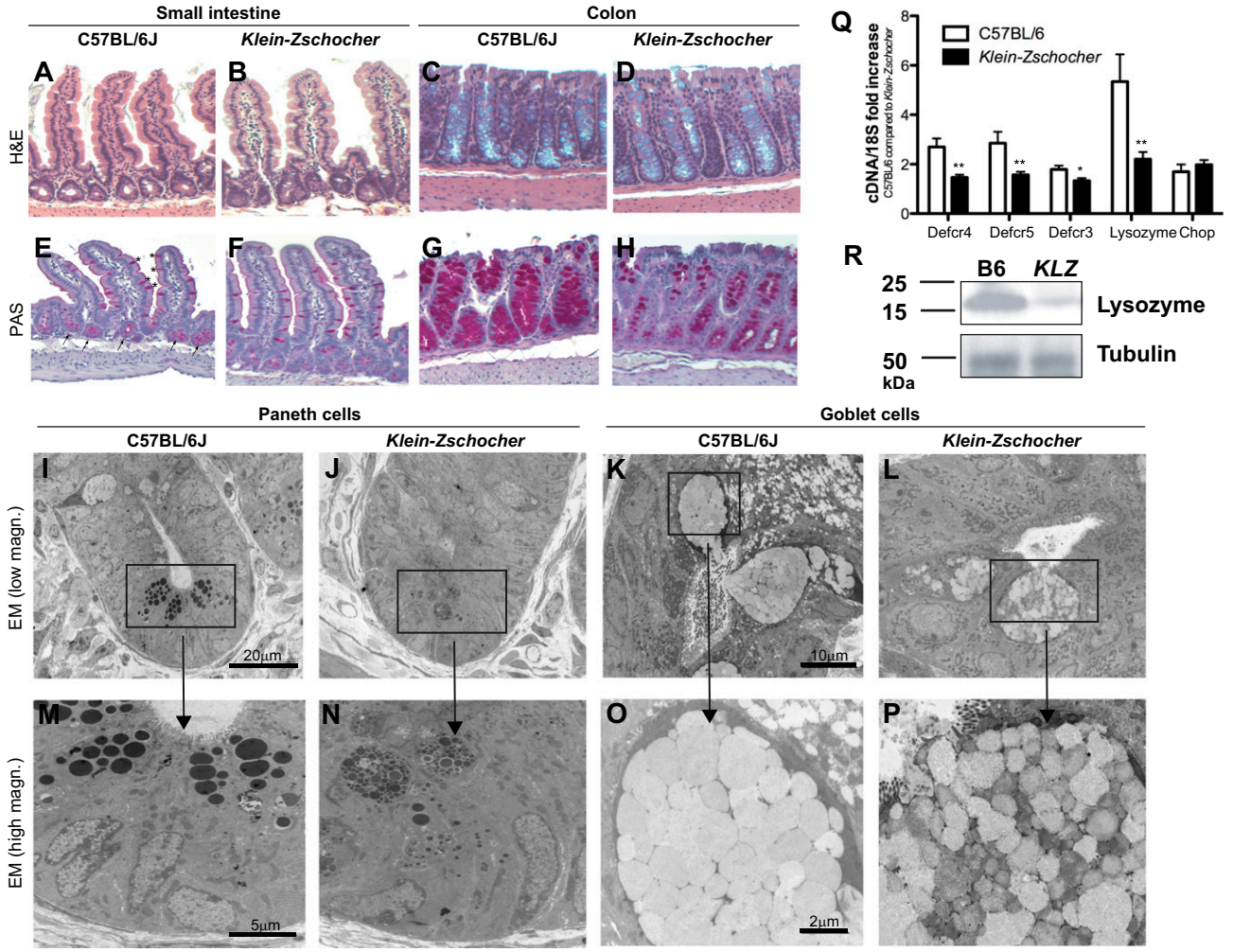

Fig. 2. Aberrant morphology of Paneth and goblet cells of *Klein-Zschocher* mice. H&E (*A*–*D*) and periodic acid-Schiff (PAS) staining (*E*–*H*) of small intestines and colons (magnification 200×). Arrows point to Paneth cells; asterisks are beside goblet cells. Electron microscopy of Paneth (*I*, *J*, *M*, and *N*) and goblet (*K*, *L*, *O*, and *P*) cells. (*Q*) mRNA from small intestine of WT and *Klein-Zschocher* mice analyzed for cryptdin-4 (Defcr4), cryptdin-5 (Defcr5), cryptdin-3 (Defcr3), lysozyme and Chop expression. Data are normalized to 18S, $n = 5$–8 each group, unpaired t test, $^{*}P < 0.05$, $^{**}P < 0.01$. Error bars represent SEM. (*R*) Lysozyme immunoblot of protein extracts from small intestine of WT (B6) and *Klein-Zschocher* (*KLZ*) mice. Tubulin was used as a loading control.

exon 4. cDNA sequencing revealed that the mutation results in skipping of exon 4 thereby reducing the size of an amplified fragment from 744 to 701 bp (Fig. 3*E*). Splicing of exon 3 to exon 5 creates a frameshift and a premature stop codon at position 89 (the first abnormal codon after exon 3) (Fig. 3 *D* and *E*). Capillary sequencing confirmed the hemizygous status of the mutation in all four affected male mice sequenced by SOLiD. Transgenic expression of a bacterial artificial chromosome (BAC) containing wild-type *Yipf6*, inserted at an autosomal site (Fig. S2), fully rescued the Paneth and goblet cell phenotypes and abolished DSS hypersensitivity (Fig. 3 *F* and *G*).

RT-PCR analysis using wild-type mice revealed expression of *Yipf6* at high levels throughout the gastrointestinal tract, particularly in the colon (Fig. 4*A*). Together with previous findings (7), these data support the idea that mammalian Yip1 family proteins display distinct tissue specificities. Using either Flag or Yipf6 antibodies, wild-type Yipf6 was represented by three major bands (25, 45, and 75 kDa) in immunoblot or immunoprecipitation analysis of an N-terminally Flag-tagged full-length protein (Fig. 4 *B* and *C*). A truncated Yipf6 construct corresponding to the mutant produced a band at the expected size of 11 kDa (Fig. 4 *B* and *C*). The higher molecular weight bands were not eliminated by tunicamycin treatment. As the predicted molecular mass of Yipf6 is 26 kDa, we surmise that Yipf6 is strongly self-associating, consistent with recent data indicating the interaction of yeast Yip family members and suggesting the formation of a complex (8–10).

Immunostaining of transfected HEK293 cells demonstrated colocalization of Yipf6 with the *cis*-Golgi marker GM130 and the *trans*-Golgi network marker TGN46 (Fig. 4*D* and Fig. S3*A*), consistent with previous findings (11). In addition, Yipf6 showed clear colocalization with the coat protein complex II (COPII) marker Sec31a (Fig. 4*D*), in agreement with reports on Yip function in yeast. In contrast, Yipf6 failed to colocalize with the mitochondrial marker MTC02 (Fig. 4*D*) and with the ER marker Kdel (Fig. S3*B*). Yipf6 thus appears to transit the Golgi compartments and may function at any location therein. Because the granules of Paneth and goblet cells are significantly smaller in *Klein-Zschocher* hemizygotes than in wild-type mice, we propose that Yipf6 has an important role in membrane transport or vesicle fusion in the *trans*-Golgi compartment, likely in a cell-type–delimited manner.

Yipf6 is one of seven members of the Yip1 gene family first described in *Saccharomyces cerevisiae*, and thought to regulate Rab protein-mediated ER-to-Golgi membrane transport (8). Notably, we observed swollen ER in pancreatic acinar cells, which

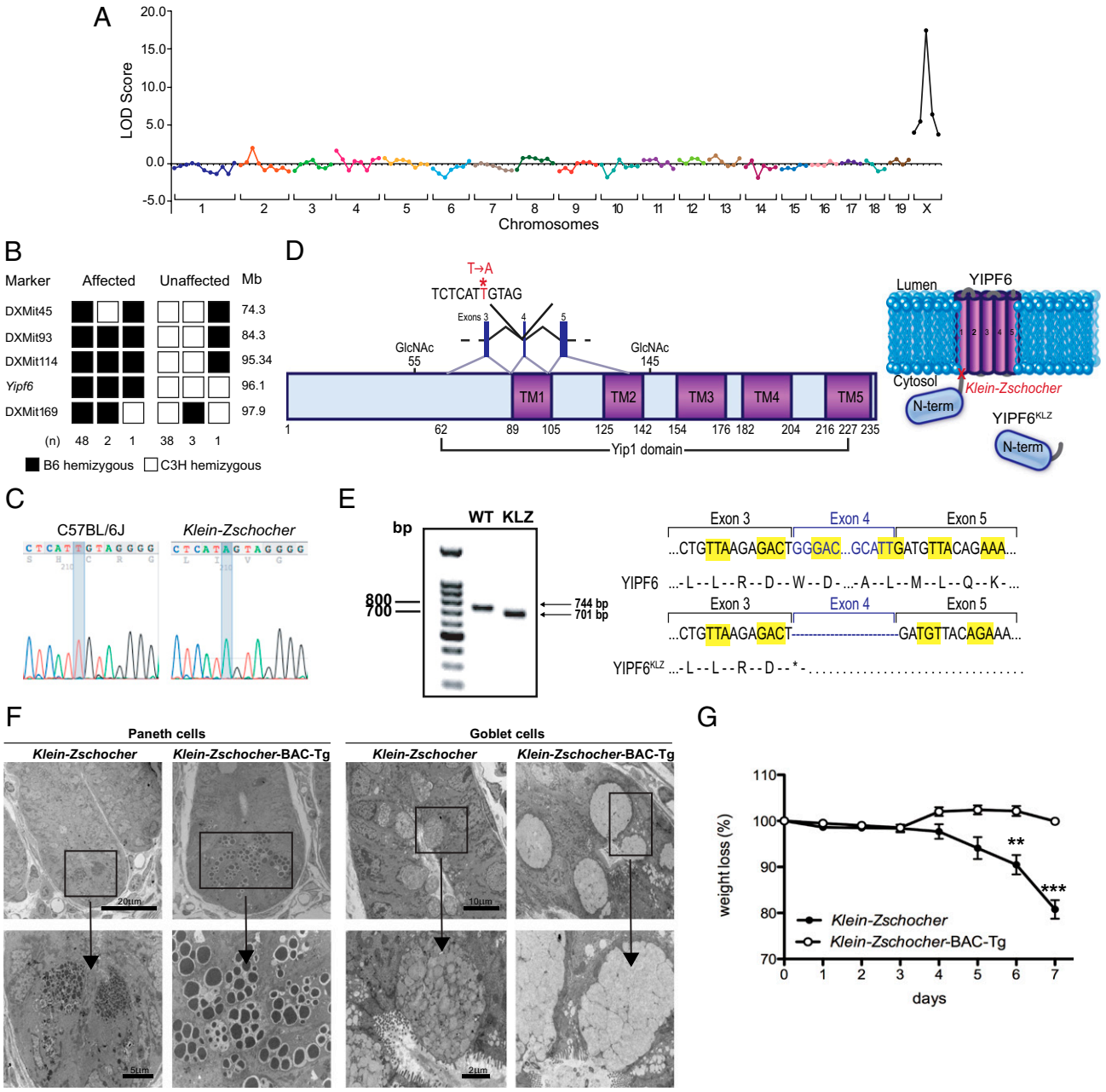

Fig. 3. The *Klein-Zschocher* phenotype is caused by a mutation of *Yipf6*. Chromosomal mapping (*A*) and fine mapping (*B*) of the *Klein-Zschocher* phenotype. LOD, logarithm of odds score; Mb, megabases. (*C*) DNA sequence chromatograms showing the mutated nucleotide in *Yipf6*. (*D*) Predicted domain and topographic organization of Yipf6. KLZ, *Klein-Zschocher*; TM, transmembrane domain (*E*) cDNA sequence of fragments of WT (744 bp) and mutant *Yipf6* (701 bp) amplified across exons 2-5. *, stop codon. (*F*) Electron microscopy of Paneth and goblet cells from *Klein-Zschocher* and *Klein-Zschocher* BAC transgenic mice. (*G*) Percent weight change of *Klein-Zschocher* and *Klein-Zschocher* BAC transgenic mice that received 1% DSS in the drinking water for 7 d. n = 3–7 each group, unpaired t test, $^{**}P < 0.01$, $^{***}P < 0.001$. Error bars represent SEM.

did not cause overt disease (Fig. S4). Together with the colocalization of mouse Yipf6 and Sec31a, this observation suggests that Yipf6 may indeed be required for efficient membrane transport from ER to Golgi via COPII vesicles, at least in acinar cells.

Our findings suggest a specific and essential function for Yipf6 in granule secretion by Paneth and goblet cells of the intestinal tract, and a consequent role in the maintenance of intestinal homeostasis in mice. Because mouse mutations that cause DSS hypersensitivity have predicted intestinal inflammation in humans (1, 5, 12–18) and particularly because the null allele of *Yipf6* described here causes spontaneous disease, we suggest that *YIPF6* should be regarded as a susceptibility locus when searching for causes of IBD in humans.

Materials and Methods

ENU Mutagenesis. C57BL/6J and C57BL/6J Ly5.1 congenics were purchased from The Jackson Laboratories. All mice were housed in The Scripps Research Institute vivarium. All animal procedures were approved and performed according to The Scripps Research Institute guidelines for animal care. C57BL/6J mice were used for ENU mutagenesis to generate the *Klein-Zschocher* strain, as described at http://mutagenetix.utsouthwestern.edu/home.cfm. The *Klein-Zschocher* strain (C57BL/6J-*Yipf6*^{m1Btlr}/Mmucd; 034313-UCD) has been deposited and is available at the Mutant Mouse Regional Resource Center.

Mapping and Sequencing. *Klein-Zschocher* males were mated to C3H/HeN females (Taconic), and the offspring backcrossed to the index mouse.

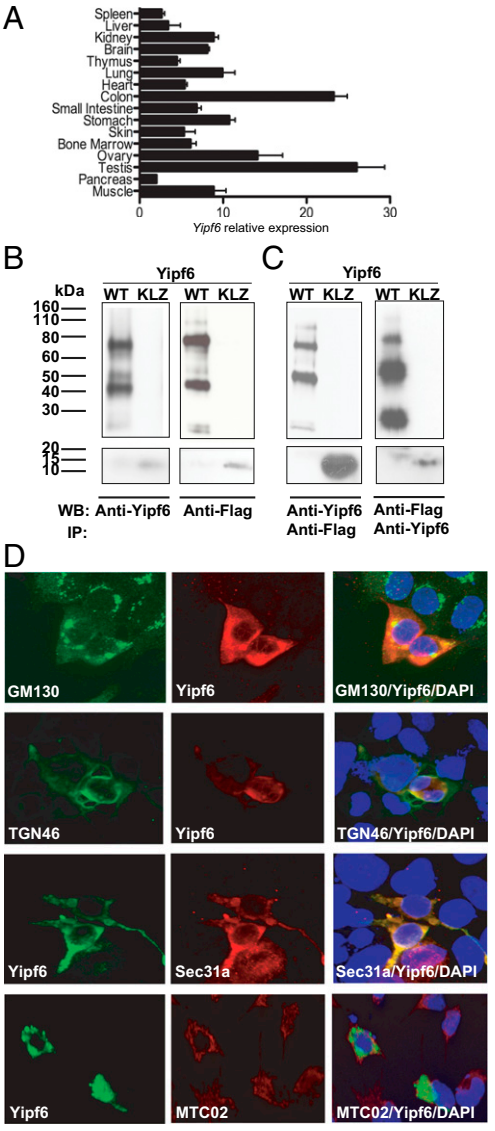

Fig. 4. Yipf6 is mainly expressed in the intestinal tract and localizes with Golgi markers and COPII coat protein. (*A*) mRNA levels of Yipf6 in different tissues. Error bars represent SEM. (*B*) Detection of wild-type Yipf6 (*Upper*) or the truncated mutant protein (*Lower*) in transfected HEK293 cells with Flag antibody or with a rabbit polyclonal antibody raised against the N-terminal domain of Yipf6. KLZ, *Klein-Zschocher*. (*C*) Immunoprecipitation of wild-type Yipf6 (*Upper*) or the truncated mutant protein (*Lower*) from transfected cell lysates using anti-Flag beads or using biotinylated Yipf6 antibody followed by streptavidin beads. (*D*) Localization by confocal microscopy of murine Yipf6 protein in HEK293 cells transfected with Flag-Yipf6 construct. Cells were stained with polyclonal Yipf6 antibody along with antibodies for the Golgi markers GM130 and TGN46, COPII coat protein Sec31a, and the mitochondrial marker MTC02. Nuclei were stained with Hoechst 33342 (magnification 600×).

The progeny were phenotyped and genotyped for mapping by analyzing 128 microsatellites markers in genome-wide linkage analysis. For high-resolution mapping, four additional markers were used as indicated in Fig. 3*B*. Genomic DNA from four male *Klein-Zschocher* mice was used to create a fragment library for four slides of whole-genome sequencing on the SOLiD 3 (two slides) and SOLiD 4 (two slides) platforms (Applied Biosystems). Whole-genome sequencing of four slides yielded 88.4% coverage of nucleotides in coding regions and splice junctions with three or more reads.

Transgenesis. The BAC clone RP23-283G14 (of C57BL6/J origin), which represents a genomic DNA fragment between positions 96107717 bp and 96309506 bp on chromosome X, was obtained from BAC-PAC. *Stard8*, the only other gene also included in the BAC, was sequenced with 100% coverage of coding regions in *Yipf6*$^{Klz/Klz}$ DNA and no mutations were found. After purification (alkaline lysis), the genomic DNA was microinjected into the male pronucleus of fertilized *Klein-Zschocher* oocytes. Approximately 600 embryos were transferred to pseudopregnant CD1 females, which gave birth to 129 pups. A single transgenic founder was identified among weanlings by sequencing genomic DNA amplified across the *Klein-Zschocher* mutation site.

DSS-Induced Colitis. For screening and phenotyping of the *Klein-Zschocher* stock, sex- and age-matched littermates received 1% DSS (MP Biomedicals) in the drinking water for 7 d. Weight was recorded daily. Mice that gained more than 10% of their initial weight were excluded from the screen. For survival analysis 4% DSS in the drinking water was used.

Constructs, PCR, and Transfections. cDNA containing full-length Yipf6 was cloned from CT26 cells. To obtain Flag-Yipf6 or Flag-Yipf6^{Klz}, a primer containing the Flag-tag sequence was used (for wild-type Yipf6: 5′ TAAAGCTTATGGACTACAAAGACGATGACGACAAGGCGGAAGCGGAGGACTCTCC and 3′ TACTCGAGTCATGGCGTGAACGTGAGTATC; for Yipf6^{Klz}: 5′ TAAAGCTTATGGACTACAAAGACGATGACGACAAGGCGGAAGCGGAGGACTCTCC and 3′ TACTCGAGTCAGTCTCTTAACAGTGCATTACTC). Both products were cloned into the expression vector pCDNA3.1 mycHisB with the restriction sites HindIII and XhoI. For cDNA sequencing of wild-type and mutant Yipf6, RNA was isolated from intestinal epithelial cells, cDNA was obtained as described below. The following primer pair was used: 5′ GCGTCCCCAAACAGTGAGCAAATAG and 3′ ATTGGTCCCTGTCCAGCCAAAAG. Yipf6-GFP plasmid was purchased from Origene (MG202877). Kdel-GFP construct (a kind gift from Kanagaraj Subramanian, The Scripps Research Institute) was generated by inserting calreticulin signal peptide (1–18 aa) sequence at the N-terminus of GFP in pEGFP-N1 vector (Clontech) and incorporating ER retention signal KDEL sequence at the C-terminal region of GFP with stop codon by seamless cloning.

For transfection experiments, HEK 293 cells were transfected with 10 μg of the indicated plasmid using Fugene HD (Roche) according to the manufacturer's instructions. After 3 d cell lysates were prepared using RIPA lysis buffer. For confocal microscopy, cells were transfected for 12–24 h.

Electron Microscopy. Mice were exsanguinated with 0.9% saline followed by perfusion fixation with 4% paraformaldehyde, 1.5% glutaraldehyde, and 0.02% picric acid in 0.1 M cacodylate buffer and, following dissection of selected pieces of gut tissues, continued overnight immersion fixation at 4 °C. The tissues were then buffer washed, postfixed in 1% osmium tetroxide, and subsequently dehydrated in graded ethanol series, transitioned in propylene oxide, and embedded in EMbed 812/Araldite (Electron Microscopy Sciences). Thick sections (1 μm) were cut, mounted on glass slides, and stained in toluidine blue for general assessment in the light microscope. Subsequently, 70-nm thin sections were cut with a diamond knife (Diatome), mounted on copper slot grids coated with parlodion, and stained with uranyl acetate and lead citrate for examination on a Philips CM100 electron microscope (FEI). Images were documented using a Megaview III CCD camera (Olympus Soft Imaging Solutions).

Histology and Immunohistochemistry. Freshly isolated small intestine or colon was fixed in formalin and embedded in paraffin. Hematoxylin–eosin staining was conducted using a standard protocol. Periodic acid-Schiff (PAS) stain was performed using PAS kit from Sigma according to the manufacturer's instructions.

Confocal Microscopy. Following transfection, HEK 293 cells were washed in PBS and fixed in 4% electron microscopy-grade formaldehyde (Polysciences) in PBS for 10 min. Cells were permeabilized and blocked with 0.1% Triton X-100, 1 mg/mL BSA, 3% goat serum, 1 mM EDTA (pH 8) in PBS for 1 h. Cells were then incubated with primary antibody (GM130, BD Biosciences; TGN46, Novus Biologicals; MTC02, Abcam; and Sec31a, BD Biosciences) overnight and subjected to staining with secondary antibody (all Invitrogen) for 30 min. Coverglasses were mounted onto slides with ProLong Gold antifade reagent (Invitrogen). Negative controls were performed by omitting the primary antibodies.

Samples were viewed using a Rainbow Radiance 2100 laser scanning confocal system attached to a Nikon TE2000-U inverted microscope (Bio-Rad–Zeiss). Images were acquired using Laser Sharp 2000 software and then imported and further analyzed using ImageJ (National Institutes of Health Imaging; http://rsb.info.nih.gov/ij).

Real-Time PCR Analysis. RNA from distal small intestine was isolated using TRIzol reagent (Invitrogen). DNase-treated RNA underwent randomly primed cDNA synthesis and real-time PCR analysis. SYBR Green-based real-time PCR was performed using the DyNAmo SYBR Green qPCR kit (Finnzymes). Primers were designed using National Institutes of Health qPrimerdepot software. For Yipf6 expression analysis, RNA from indicated tissue was isolated as described above (Yipf6 primer: 5′ GTAATGCACTGTTAAGAGACT, 3′ CGCCATCATTCTTCCCATCAA). All signals were normalized to 18S. Normalized data were used to measure relative expression levels of different genes using ΔΔCt analysis.

Western Blot Analysis. Small intestines were flushed with PBS and a distal piece (0.5 cm) was homogenized in RIPA buffer. Protein content was determined by BCA assay (Pierce), and protein samples were analyzed by reducing 4–20% Mini-Protean TGX precast gels (Bio-Rad) and detected with lysozyme (Santa Cruz), LC3B (Novus Biologicals) and tubulin (Santa Cruz) antibodies.

For detection of Flag-Yipf6 or Flag-Yipf6^{Klz} anti-Flag antibody M2 (Sigma) or a rabbit polyclonal antibody against the N-terminal segment (peptide [H]-ClPSRARAQEHDSSTLNESIR-[NH2] was used as an immunogen) of Yipf6 was used. This antibody and also the biotinylated form were generated by Covance.

Generation of BM Chimeric Mice. Generation of BM chimeric mice was performed as described (19–21). Recipient WT (CD45.1) or *Klein-Zschocher* (CD45.2) mice were lethally irradiated with 950 rads using a ^{137}Cs source and injected i.v. 2–3 h later with 5×10^6 BM cells derived from the tibia and femurs of the respective donors. Seven weeks after engrafting, reconstitution was assessed by FACS analysis of peripheral blood. Cells were stained with FITC-labeled CD45.1 antibody and PerCPCy5.5-labeled CD45.2 antibody and cell suspensions were analyzed on a BD Biosciences FACSCalibur.

FITC Dextran Permeability Assay. Intestinal permeability was assessed by luminal enteral administration of FITC-dextran 4000 (Sigma), a nonmetabolizable macromolecule that is used as a permeability probe. All mice were gavaged with FITC-dextran (40 mg/100 g body weight) 4 h prior to killing. Whole blood was obtained by retroorbital bleeding and FITC-dextran measurements were performed in duplicate by fluorometry. Dilutions of FITC-dextran in PBS were used as a standard curve, and absorption of 100 μL serum or standard measured in a fluorimeter at 488 nm.

Statistical Analysis. Statistical analysis was performed using GraphPad Prism software. All differences with P values <0.05 were considered significant.

ACKNOWLEDGMENTS. The authors thank M. Wood from the Core Microscopy Facility at The Scripps Research Institute for assistance with electron microscopy and D. La Vine for help with illustrations. This research was supported by the Crohn's and Colitis Foundation through a career development award (to K.B.) and by National Institutes of Health Broad Agency Announcement Contract HHSN27220000038C.

1. Brandl K, et al. (2010) MyD88 signaling in nonhematopoietic cells protects mice against induced colitis by regulating specific EGF receptor ligands. *Proc Natl Acad Sci USA* 107:19967–19972.
2. Thiagarajah JR, Zhao D, Verkman AS (2007) Impaired enterocyte proliferation in aquaporin-3 deficiency in mouse models of colitis. *Gut* 56:1529–1535.
3. Brandl K, et al. (2009) Enhanced sensitivity to DSS colitis caused by a hypomorphic Mbtps1 mutation disrupting the ATF6-driven unfolded protein response. *Proc Natl Acad Sci USA* 106:3300–3305.
4. Heazlewood CK, et al. (2008) Aberrant mucin assembly in mice causes endoplasmic reticulum stress and spontaneous inflammation resembling ulcerative colitis. *PLoS Med* 5:e54.
5. Kaser A, et al. (2008) XBP1 links ER stress to intestinal inflammation and confers genetic risk for human inflammatory bowel disease. *Cell* 134:743–756.
6. Cadwell K, et al. (2008) A key role for autophagy and the autophagy gene Atg16l1 in mouse and human intestinal Paneth cells. *Nature* 456:259–263.
7. Tang BL, et al. (2001) A membrane protein enriched in endoplasmic reticulum exit sites interacts with COPII. *J Biol Chem* 276:40008–40017.
8. Yang X, Matern HT, Gallwitz D (1998) Specific binding to a novel and essential Golgi membrane protein (Yip1p) functionally links the transport GTPases Ypt1p and Ypt31p. *EMBO J* 17:4954–4963.
9. Ito T, et al. (2001) A comprehensive two-hybrid analysis to explore the yeast protein interactome. *Proc Natl Acad Sci USA* 98:4569–4574.
10. Calero M, Winand NJ, Collins RN (2002) Identification of the novel proteins Yip4p and Yip5p as Rab GTPase interacting factors. *FEBS Lett* 515:89–98.
11. Shakoori A, et al. (2003) Identification of a five-pass transmembrane protein family localizing in the Golgi apparatus and the ER. *Biochem Biophys Res Commun* 312: 850–857.
12. Brandl K, Tomisato W, Beutler B (2012) Inflammatory bowel disease and ADAM17 deletion. *N Engl J Med* 366:190–, author reply 190.
13. Blaydon DC, et al. (2011) Inflammatory skin and bowel disease linked to ADAM17 deletion. *N Engl J Med* 365:1502–1508.
14. Esworthy RS, et al. (2001) Mice with combined disruption of Gpx1 and Gpx2 genes have colitis. *Am J Physiol Gastrointest Liver Physiol* 281:G848–G855.
15. Hammer RE, Maika SD, Richardson JA, Tang JP, Taurog JD (1990) Spontaneous inflammatory disease in transgenic rats expressing HLA-B27 and human beta 2m: An animal model of HLA-B27-associated human disorders. *Cell* 63:1099–1112.
16. Kühn R, Löhler J, Rennick D, Rajewsky K, Müller W (1993) Interleukin-10-deficient mice develop chronic enterocolitis. *Cell* 75:263–274.
17. Takeda K, et al. (1999) Enhanced Th1 activity and development of chronic enterocolitis in mice devoid of Stat3 in macrophages and neutrophils. *Immunity* 10:39–49.
18. Welte T, et al. (2003) STAT3 deletion during hematopoiesis causes Crohn's disease-like pathogenesis and lethality: A critical role of STAT3 in innate immunity. *Proc Natl Acad Sci USA* 100:1879–1884.
19. Brandl K, et al. (2008) Vancomycin-resistant enterococci exploit antibiotic-induced innate immune deficits. *Nature* 455:804–807.
20. Brandl K, Plitas G, Schnabl B, DeMatteo RP, Pamer EG (2007) MyD88-mediated signals induce the bactericidal lectin RegIII gamma and protect mice against intestinal Listeria monocytogenes infection. *J Exp Med* 204:1891–1900.
21. Sansonetti PJ (2004) War and peace at mucosal surfaces. *Nat Rev Immunol* 4:953–964.